

Article

Effect of the N/C Ratios of Ammonia Added to Process Gas Mixtures on the Morphology and Structure of MPCVD Diamond Films

Xuejie Liu *, Hongchao Wang, Pengfei Lu, Yuan Ren, Xin Tan, Shiyang Sun and Huiling Jia

School of Mechanical Engineering, Inner Mongolia University of Science and Technology, Arding Str. No. 7, Baotou 014010, China; wanghcskye@163.com (H.W.); lupengfei1005@163.com (P.L.); renyuan_bt@126.com (Y.R.); heart_tan@126.com (X.T.); sunshy@imust.cn (S.S.); hljia@imust.cn (H.J.)

* Correspondence: liuxuejie@imust.edu.cn; Tel./Fax: +86-472-595-2268

Received: 19 March 2018; Accepted: 23 April 2018; Published: 27 April 2018



Abstract: In this study, N-doped diamond films were prepared through microwave plasma chemical vapor deposition with $\text{NH}_3/\text{CH}_4/\text{H}_2$ gas mixtures. The effects of the ammonia addition to the process gas mixture on the morphology and structure of diamond films were systematically investigated through characterization by scanning electron microscopy (SEM), atomic force microscopy (AFM), X-ray diffraction (XRD), Raman spectroscopy, and X-ray photoelectron spectroscopy (XPS). This work focuses on the ammonia addition to the process gas mixtures in the narrow range of N/C ratios from 0.4% to 1.0%. The results reveal that different N/C ratios can affect the morphology, the preferred crystal orientation, and the sp^3/sp^2 ratio in the films. When the N/C ratio of the process gas mixture ranges from 0.6% to 1.0%, the XRD and SEM results show that ammonia addition is beneficial for the growth of the (110) faceted grains. When the N/C ratio of the process gas mixture ranges from 0.8% to 1.0%, the XPS and Raman results indicate that the diamond films exhibit a considerable enhancement in the sp^3 fraction.

Keywords: ammonia doping; diamond films; MPCVD; morphology; diamond quality

1. Introduction

Nitrogen (N)-doped diamond films have been studied for their many applications, such as in semiconductor devices [1], thermionic electron emission [2], photoelectron emission [3], field emission [4], electrochemical biosensing [5], sterilization [6], and N-V color centers for quantum communications [7]. The performance of N-doped diamond films strongly depends on the film microstructure. Thus, many studies have investigated the effects of N addition on the growth and structure of diamond films. The findings of the studies indicate that N addition can lead to a high growth rate of the films [8–10], but a low deposition efficiency [11,12]. However, many different results have been reported regarding the influence of N addition on the film morphology and the diamond quality, with reports of N addition benefiting the growth of the (100) facet surface [9,11,13–18], producing films without any preferred orientation of the surface facets [12,19,20] and improving diamond quality [13,16,21] or leading to a higher sp^2 fraction in the deposited material [19,20]. These different results are highly dependent on the process parameters and the N/C atomic ratio in the process gas mixture. Although many experimental studies have been conducted on this subject, the effects of N addition on the morphology, microstructure, and quality of N-doped diamond films warrant further study. Drawing on the experience of previous studies of a broad range of N/C atomic ratios (0.1%, 1.0%, 10.0%, and 40%) [11] and of very low N/C ratios (from 0.02% to 0.32%) [19], this work focuses on the ammonia addition to process gas mixtures in a narrow N/C ratio range from 0.4% to 1.0%.

In our previous studies, first-principles calculations were conducted to investigate the adsorption and migration behaviors of Si, B, Y, Nb, and Ti doped on diamond surfaces [22–27]. The purpose of our research is to study the modification effects of the doping elements on diamond films and to further develop new types of doped diamond films. The calculations of the adsorption and migration behaviors of Si and B atoms on diamond surfaces suggest that the number and distribution of open radical sites can affect the growth of diamond films [23,24]. Recently, we studied Ti-doped diamond films on which the Ti was deposited by microwave plasma chemical vapor deposition (MPCVD) [27]. The results of this study indicate that Ti doping can influence the morphology and microstructure of diamond films. Our research shows that the film morphology and the sp^3 phase fraction warrant an in-depth investigation.

To study the species participating in the film growth process, Ashfold's group systematically investigated N_2/H_2 , NH_3/H_2 , and $CH_4/N_2/H_2$ plasmas in the N-doped diamond deposition process [28–30]. This group's results show that compared to the addition of N_2 to the process gas, the inclusion of NH_3 to feed gas may introduce more reactive species to the film growth process. Therefore, in this study, N-doped diamond films were synthesized through the MPCVD process using an ammonia-containing gas mixture. First, a diamond film with a (110) facet surface was prepared by adjusting the process parameters. Second, under the same process conditions, N-doped diamond films were synthesized by adding various ammonia dopant fluxes to the process gas mixture. After the deposition process was complete, scanning electron microscopy (SEM), atomic force microscopy (AFM), X-ray diffraction (XRD), micro-Raman spectroscopy, and X-ray photoelectron spectroscopy (XPS) were conducted to investigate the effects of N doping on the microstructure, surface morphology, and quality of the diamond films.

2. Experiment Details

Diamond films and N-doped diamond films were deposited via MPCVD. Single-crystalline (100) silicon wafers were used as substrates and were pretreated before the deposition. First, the wafers were abraded manually with diamond powder and titanium powder for 15 min. Second, the wafers were placed in anhydrous acetone with a diamond powder and titanium powder suspension for a 20-min ultrasonic abrasion step to enhance the seed density. Third, the wafers were ultrasonically cleaned in anhydrous ethanol for 20 min.

In the film deposition experiment, the microwave power was 1.5 kW, the work pressure was maintained at approximately 5.4 kPa, and the temperature of the substrate was 850 °C. The deposition time of all films was 4 h. A bias voltage (−50 V) was added to the substrate to enhance the nucleation. The flow rates of methane (CH_4), hydrogen (H_2), and ammonia (NH_3) were precisely controlled by mass flow controllers. Hydrogen and 1.0% methane were the process gases for the diamond film deposition. Ammonia diluted to 0.1% using hydrogen was used as the N source. The flow rates of the diluted ammonia gas were 12, 18, 24, and 30 sccm. The N/C atomic ratios in the feed gas ranged between 0.4% and 1%.

The morphology, grain sizes, and surface roughness of the films were evaluated by SEM (QUANTA 400, FEI, Hillsboro, OR, USA) and AFM (Dimension Edge, Bruker, Karlsruhe, Germany). The preferential orientation of the crystals in the films was investigated by transposable polycrystalline XRD (D8 ADVANCE) at 2θ angles ranging from 40° to 145° with a scan speed of 2°/min. The light source emitted by the Cu $K\alpha$ tube was flashing infrared with a power of 1600 W. The detector slits were 1.0 mm and 0.2 mm wide, and the Ni filter was placed in the middle. The quality of the diamond samples was analyzed using Raman spectroscopy (XploRA Raman Microscope, HORIBA Jobin Yvon, Kyoto, Japan) at an excitation wavelength of 532 nm. Compositional and quantification analyses were conducted using XPS (ESCALAB 250XI, Thermo Fisher, Waltham, MA, USA) with Al $K\alpha$ (1500 W).

Due to the nature of the MPCVD method, for a definite diamond film sample that had undergone deposition, the morphology at the sample center was somewhat different from that in the surrounding areas. Therefore, for comparison, the centers of all samples were selected as the measurement locations.

3. Results and Discussion

3.1. Effect of Nitrogen on the Film Morphology

The SEM images of the N-doped diamond films deposited with different N/C ratios in the process gas mixtures are shown in Figure 1. These micrographs show a remarkable modification in the film morphology after ammonia was added into the $\text{CH}_4 + \text{H}_2$ gas mixture. The morphology of the undoped diamond film shows two kinds of crystallites. Large grains show (110) oriented facets with clear and sharp boundaries, thereby forming pyramid-shaped crystals, as shown in Figure 1a. Small nanometer-sized grains surround the large grains and have an unclear orientation. Upon the addition of ammonia into the process gas mixture with a low N/C ratio of 0.4%, the film morphology significantly changes and becomes cauliflower-like. As shown in Figure 1b, large grains are covered with nanocrystalline grains, which is typical for nanocrystalline diamond films [19]. By increasing the ammonia flux to a 0.6% N/C ratio, the surface becomes flat, and elevated sections or ridges begin to appear as obvious square facets (Figure 1c). With a further increase in the ammonia flux to a 0.8% N/C ratio, more (110) facet grains appear on the surface [Figure 1d] compared to the case shown in Figure 1c. Upon a further increase in the ammonia flux to a 1.0% N/C ratio, the morphology of the surface is filled with (110) facet grains (Figure 1e). Generally, ammonia addition to the process gas mixture can significantly influence the film morphology and the preferred orientation of the crystals. For N/C ratios from 0.6% to 1.0% in the process gas mixture, ammonia addition is beneficial for the growth of the (110) faceted grains.

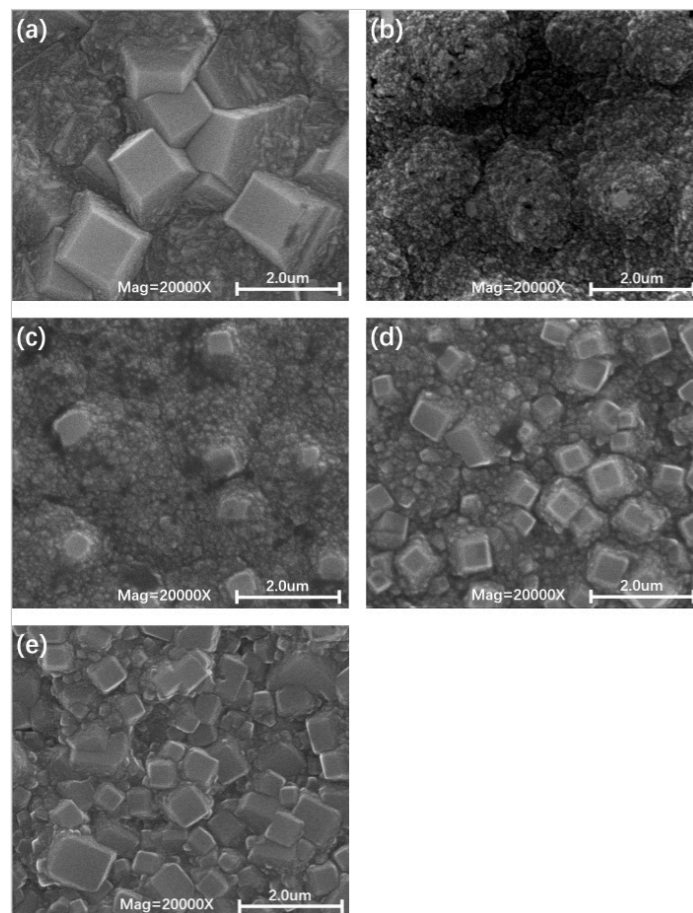


Figure 1. SEM images of diamond films deposited with various ratios of N/C in the process gas mixtures: (a) N/C = 0%, (b) N/C = 0.4%, (c) N/C = 0.6%, (d) N/C = 0.8%, and (e) N/C = 1.0%.

3.2. AFM Analysis

The surface morphology and roughness of the samples were investigated by AFM topography analysis. The topography of the undoped diamond films shows many large, smooth cubic facets (Figure 2a). The calculated average roughness (R_a) obtained from the AFM topography analysis is approximately 131 nm. The diamond film deposited by a process gas mixture with ammonia addition at a 0.4% N/C ratio has a cauliflower-like structure (Figure 2b), and the surface roughness decreases sharply to $R_a = 75$ nm. Upon increasing the N/C ratio to 0.6%, the surface is covered with nanocrystalline grains, as shown in Figure 2c, and the surface roughness reaches its lowest value of 57 nm. With a further increase in the ammonia flux to a 0.8% N/C ratio, the film presents several columnar structures (Figure 2d) and its surface roughness reaches 78 nm. Upon a further increase of the ammonia flux to a 1.0% N/C ratio, the film surface shows many small, smooth square facets (Figure 2e), and its roughness reaches 62 nm. Overall, the film surface roughness can be reduced by ammonia addition to the process gas mixture. However, this reduction is not proportional to the ammonia flux increase.

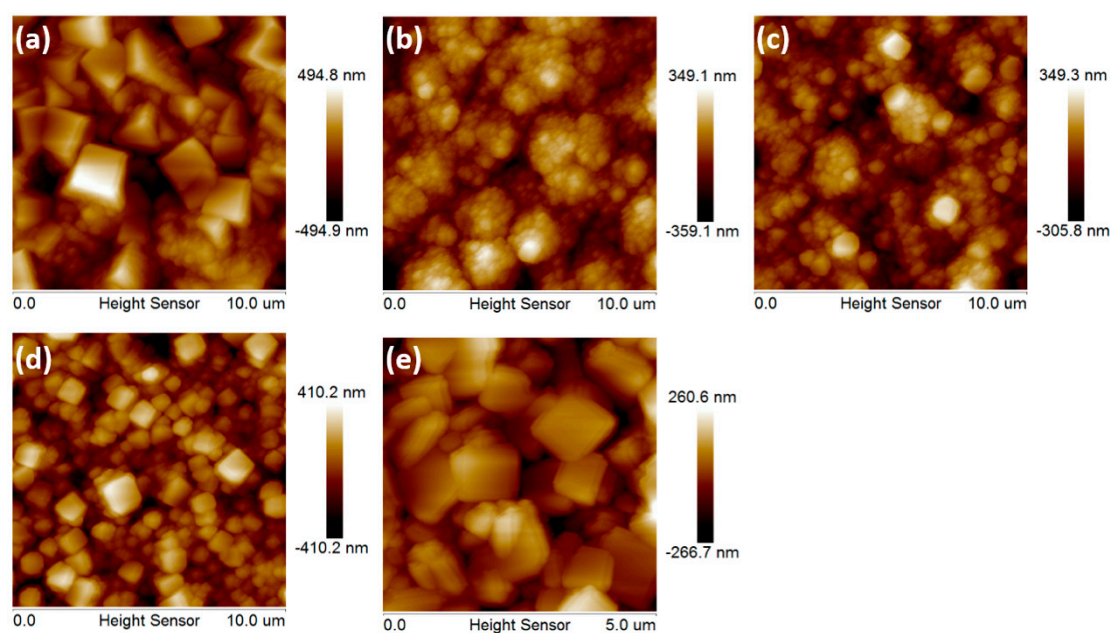


Figure 2. AFM topographies of diamond films deposited with various N/C ratios in the process gas mixtures: (a) N/C = 0%, (b) N/C = 0.4%, (c) N/C = 0.6%, (d) N/C = 0.8%, and (e) N/C = 1.0%.

3.3. X-ray Diffraction

XRD analysis was conducted to study the influence of the various ammonia additions on the crystalline structure and solid phase composition of the diamond film. Figure 3 shows the XRD patterns of the diamond films with various gas mixtures. The preferred orientation of the diamond films can be indicated by the increased intensity of the plane reflection [31]. The spectra in the 2θ range of 64° to 74° are excluded due to the strong Si diffraction peak. The characteristic diffraction peaks of diamond at 43.9° , 75.3° , 91.5° , 120° and 140° are identified as diamond (111), (220), (311), (400), and (331) diffraction peaks, respectively. The diffraction peaks correlated with the (400) and (331) planes at high 2θ angles are negligible, as shown in Figure 3, thereby revealing that the (400) and (331) facets are almost entirely absent. The intensity ratios of the (220) to (111) peaks [$I_{(220)}/I_{(111)}$] of the diamond films and the N-doped diamond films extracted from the XRD spectra are listed in Table 1. The preferred orientations of the crystals in the undoped diamond film are (111) and (220). The [$I_{(220)}/I_{(111)}$] intensity ratio is 19.0%, indicating that the (111) diamond facets are dominant in the deposited film, as shown in Figure 3a. Therefore, the small grains shown in Figure 1a should be the (111) facets. With ammonia addition at a 0.4% N/C ratio to the process gas, the [$I_{(220)}/I_{(111)}$] intensity ratio decreases to 17.4%. By increasing the N/C ratio to 0.6%, the

$[I_{(220)}/I_{(111)}]$ intensity ratio increases to 26.1%. By further increasing the N/C ratio from 0.8% to 1%, the $[I_{(220)}/I_{(111)}]$ intensity ratio increases from 32.3% to 35.4%. The growth of the (110) oriented facet grains is enhanced by the ammonia addition to the process gas mixture, which is consistent with the SEM results. Similar results were also reported by Liu and Raabe [9].

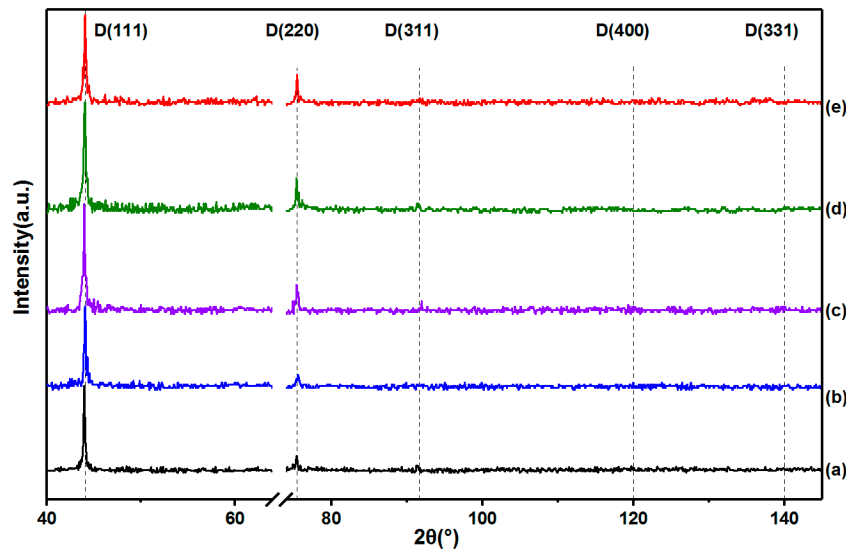


Figure 3. XRD patterns of diamond films deposited with various ratios of N/C in process gas mixtures: (a) N/C = 0%, (b) N/C = 0.4%, (c) N/C = 0.6%, (d) N/C = 0.8%, and (e) N/C = 1.0%.

Table 1. XRD patterns of diamond films deposited with various N/C ratios in process gas mixtures: (a) N/C = 0%, (b) N/C = 0.4%, (c) N/C = 0.6%, (d) N/C = 0.8%, and (e) N/C = 1.0%.

Sample	(111)		(220)		Ratio
	Position (2θ)	FWHM	Position (2θ)	FWHM	$I_{(220)}/I_{(111)}$
a	43.97	0.21	75.40	0.20	19.0%
b	43.94	0.30	75.59	0.22	17.4%
c	44.00	0.28	75.49	0.19	26.1%
d	44.05	0.17	75.45	0.21	32.3%
e	44.08	0.16	75.44	0.13	35.4%

The full width at half maximum (FWHM) of the diamond (111) and (220) XRD peaks observed at 2θ angles of 44.0° and 75.3° , respectively, can be used as a qualitative measure of the degree of crystallinity. The FWHM depends on both the grain size and the crystallinity. The FWHM tends to become narrow with large grain sizes [32]. For the undoped diamond film, the FWHMs of the (111) and (220) peaks are 0.21 and 0.20, respectively, as shown in Table 1. When the N/C ratio is 0.4%, the FWHMs of the (111) and (220) peaks increase to 0.30 and 0.22, respectively, thereby implying an increase in the nucleation rate and a decrease in the grain size of the crystals with (111) and (220) orientations, as shown in the SEM image in Figure 1b. When the N/C ratio increases to 1%, the FWHM of the (220) peak decreases to 0.13, thereby indicating the increase in the grain size of (220) oriented crystals, as shown in the SEM image in Figure 1e. This result supports the conclusion that small additions of NH_3 to the process gas influence the diamond film growth [19,33]. Overall, the preferred orientation of the crystals and the grain size can be changed by the ammonia addition into the process gas mixtures. The growth of the (110) facet grains can be promoted by a certain amount of ammonia addition. This behavior is in agreement with the SEM images presented in Figure 1e.

3.4. Raman Spectroscopy

Raman spectroscopy is a nondestructive method for investigating the vibrational band structure of materials. Figure 4 shows the Raman scattering spectra of the diamond films deposited with various ammonia additions to the process gas mixtures. The Raman scattering spectra are recorded at an excitation wavelength of 532 nm in the range of 1000 to 1800 cm^{-1} . To further study the structure of the diamond films, the Raman spectra are deconvoluted and analyzed by Gaussian contours with linear background subtraction. The diamond peak is detected at 1332 cm^{-1} , thereby indicating the existence of a diamond phase. The peaks at 1135 cm^{-1} and 1460 cm^{-1} are related to the vibrational modes of trans-polyacetylene (trans-PA) and are attributed to the C–H in-plane bending mode and the C–C, C=C stretching vibration modes, respectively [34,35]. The D-band near 1370 cm^{-1} indicates the “breathing” vibrational mode of the sp^2 -bonded carbon in the carbon rings [36]. Meanwhile, the 1540 cm^{-1} peak of the graphite G band is attributed to the in-plane stretching mode of the sp^2 -bonded carbon in the chains and rings [37]. Moreover, the peak at 1630 cm^{-1} is attributed to the characteristics of the sp^2 -hybridized composition (chains or isolated clusters) because the short and strained C=C bond chains shift the G-band to higher frequencies [35].

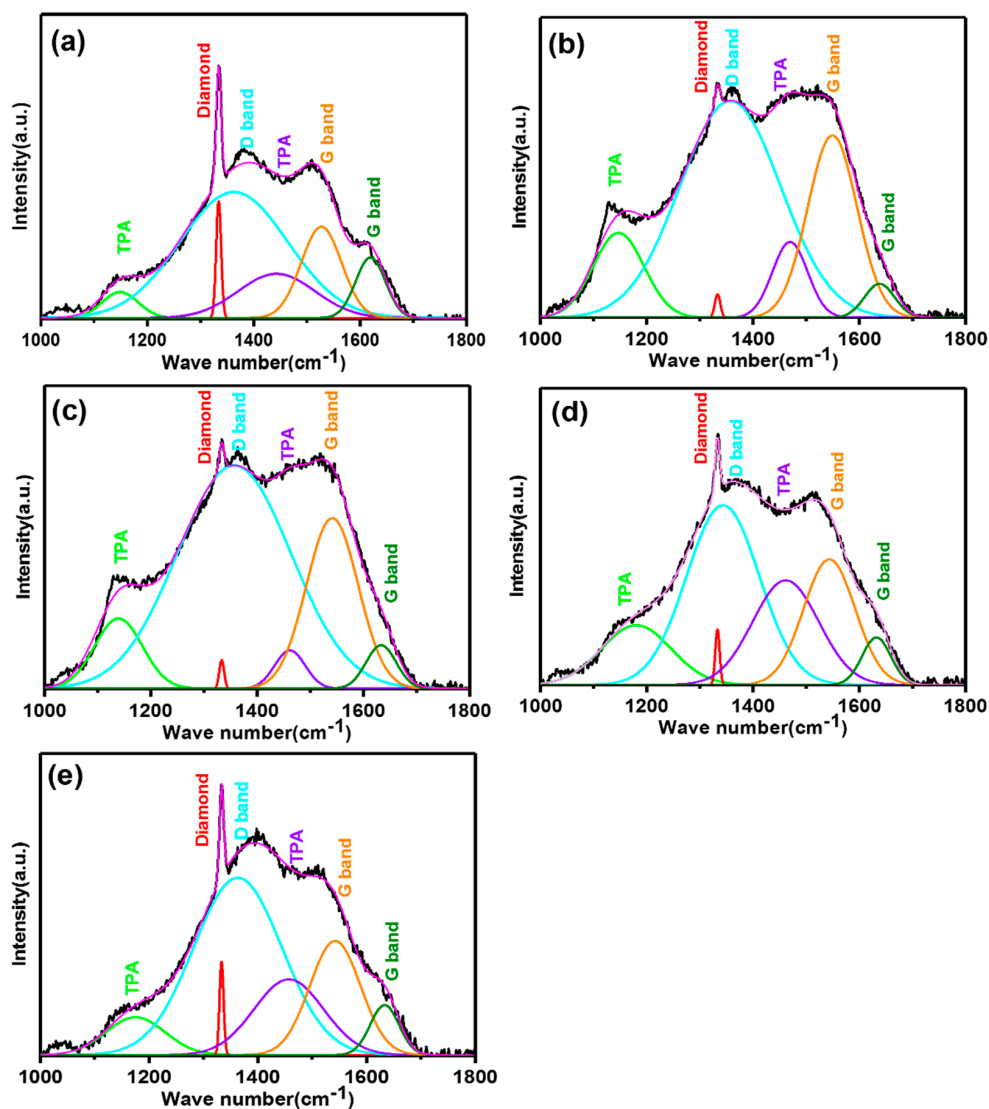


Figure 4. Gaussian fitting of Raman spectra of diamond films deposited with various N/C ratios in the process gas mixtures: (a) N/C = 0%, (b) N/C = 0.4%, (c) N/C = 0.6%, (d) N/C = 0.8%, and (e) N/C = 1.0%.

Several features of the Raman spectra of the diamond films with different amounts of added ammonia are listed in Table 2. When the N/C ratio is 0.4%, the intensity of the diamond peak is dramatically reduced, as shown in Figure 4b, while the FWHM of the diamond peak increases from 9 to 15, thereby implying a reduction in the grain size. This result is consistent with the SEM image presented in Figure 1b. When the N/C ratio increases from 0.6% to 1%, the intensities of the diamond peaks gradually increase, and the relevant FWHMs decrease accordingly. Meanwhile, the intensities of the 1135 cm^{-1} peak decrease, as shown in Figure 4b–e, thereby indicating an enhancement in the diamond phase purity. A comparison of the Raman results with the SEM and XRD results described above reveals that the quality of the diamond phase can be improved by the addition of a certain amount of ammonia into the process gas mixture.

Table 2. Raman spectra of diamond films deposited with various N/C ratios in the process gas mixtures: (a) N/C = 0%, (b) N/C = 0.4%, (c) N/C = 0.6%, (d) N/C = 0.8%, and (e) N/C = 1.0%.

Sample	Diamond Peak		G Band Peak				Ratio
	Center Position (cm^{-1})	FWHM	Center Position (cm^{-1})	FWHM	Center Position (cm^{-1})	FWHM	
a	1334	11	1527	90	1620	66	0.8
b	1333	15	1549	109	1638	67	7.8
c	1333	11	1543	115	1633	67	6
d	1333	10	1542	114	1632	64	2.3
e	1333	9	1542	110	1632	62	1.2

The diamond peak of the undoped film shifts from 1332 cm^{-1} to a higher wave number, possible because of the residual compressive stresses in the films [38,39]. When the N/C ratio is 0.4%, the diamond peak shifts to a lower frequency (1333 cm^{-1}) and remains at this frequency as the ammonia flux is further increased, thereby indicating the limited effect of ammonia addition on the adjustment of the internal stress of the film.

With the ammonia dopant flow in the process gas mixtures, the position of the G band shifts to higher frequencies, as shown in Table 2. This result shows that the grain size reduction and the increase in the grain boundary contents lead to film graphitization. As the ammonia flux increases, the position of the G band shifts to lower frequencies (from 1549 cm^{-1} to 1542 cm^{-1}). Similar trends can also be observed for the peak at 1638 cm^{-1} , indicating that the graphitization degree of the films is reduced with increasing ammonia flux. Moreover, the FWHMs of the G band related to the degree of disorder of the carbon structure initially widen before becoming narrow, thereby indicating that the structural order of the film changes with the increase in the ammonia flux. Furthermore, the change in the intensity ratio of the non-diamond and diamond fitting peak (I_n/I_d) shows the same trend as the change in the FWHM of the G band. Therefore, the crystalline structures in the deposited samples change with increasing ammonia flux.

Overall, the analysis of the Raman spectra shows that the addition of ammonia to the diamond film growth process may improve the quality of the diamond phase, while it does not remarkably influence the internal stress of the film and has a complex influence on the film graphitization.

3.5. XPS Analysis

The chemical bonding states of the diamond film and N-doped diamond films are studied based on the XPS analysis. The C 1s and N 1s spectra of the diamond films with different amounts of added ammonia are shown in Figure 5. Carbon is a non-polar atom; the bond lengths of the sp^2 -hybridized carbon are shorter than those of the sp^3 -hybridized carbon [40]. Thus, the C 1s core-energy level spectra can be deconvoluted into four bands at 284.1 eV, 284.8 eV, 285.4 eV, and 286.3 eV, which can be assigned to the sp^2 -hybridized carbon, the sp^3 bulk carbon, the $\text{sp}^3 \text{CH}_x$ ($x \geq 2$), and the C–O bonds, respectively [41,42]. The presence of oxygen atoms arises from the exposure of the samples in the air during the waiting period prior to the XPS examination. In the C 1s spectra, no clear signal is observed at 286.9 eV. Meanwhile, in the N 1s spectra, no obvious peaks are observed at 398.2 eV and 399.5 eV for the C–N bond, as shown in

Figure 6b–d. The N 1s spectrum of a 1% N/C ratio can be deconvoluted into two bands at 398.2 eV and 399.5 eV, as shown in Figure 6e, corresponding to pyridine-like and pyrrole-like nitrogen [43], which can contribute to the sp^2 C–N. According to the quantitative analysis, the N content is only 0.07%. The value is lower than the detection resolution ratio of XPS (0.1%) and it presents here as a reference. Additionally, the peak of sp^3 C–N is not observed. These observations indicate a very low and undetectable concentration of N atoms in the films. This phenomenon has also been observed in previous studies of N-doped diamond synthesis [11,12] and implies the low deposition efficiency of N addition.

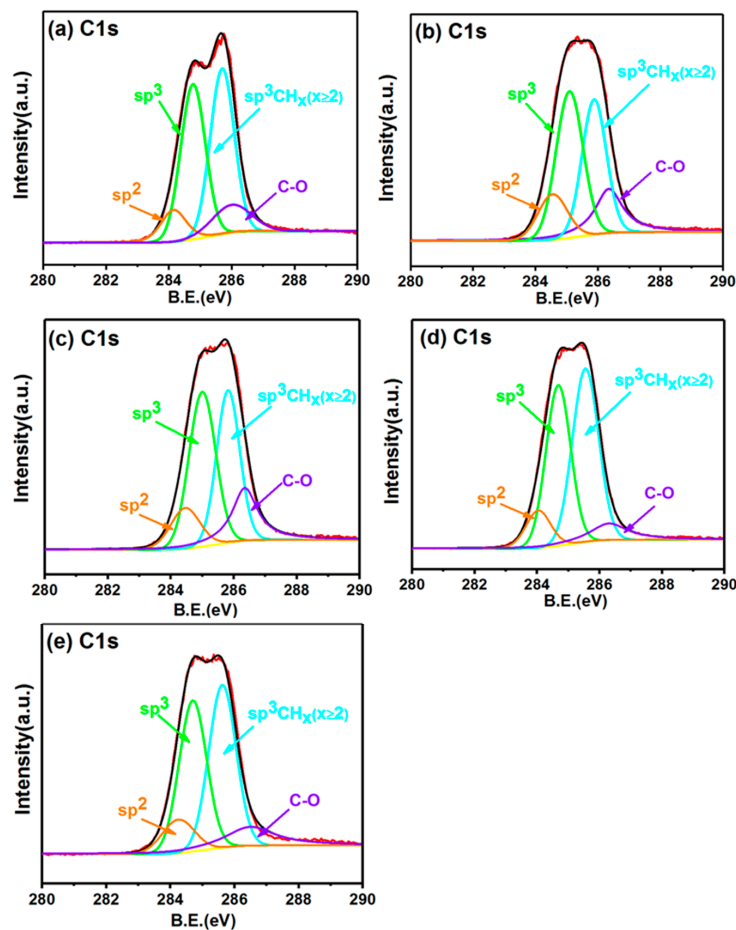


Figure 5. XPS spectra of diamond films deposited with various N/C ratios in the process gas mixtures. (a–e) C 1s spectra: (a) N/C = 0%, (b) N/C = 0.4%, (c) N/C = 0.6%, (d) N/C = 0.8%, and (e) N/C = 1.0%.

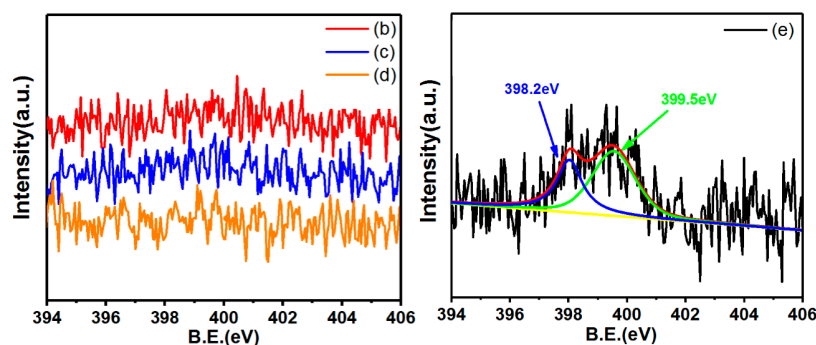


Figure 6. N 1s spectra of diamond films deposited with various N/C ratios in the process gas mixtures. (b) N/C = 0.4%, (c) N/C = 0.6%, (d) N/C = 0.8%, and (e) N/C = 1.0%.

The sp^3 -/ sp^2 -hybridization ratios are shown in Table 3 and are obtained by calculating the areas of the sp^3 and sp^2 peaks obtained by the fitting process. The sp^3/sp^2 ratio of undoped diamond film is 8.5. With the N/C ratio of 0.4%, the sp^3/sp^2 ratio of the film decreases to 5.5, indicating that the sp^2 fraction increases. Similar results were reported by Wang and co-workers [44]. The sp^2 structures are usually related to defects in the grain boundaries. The sp^2 nanocrystalline graphite phase increases due to the increased number of grain boundaries [45], which is in accordance with the SEM image [Figure 1b]. Interestingly, with an increase in the N/C ratios from 0.6% to 1%, the sp^3/sp^2 ratio of the films increases from 6.2 to 9.0. The sp^3 fraction shows an obvious increase after the ammonia addition, thereby suggesting an improvement in the quality of the diamond films. This result is consistent with the Raman analysis results.

Table 3. XPS spectra of diamond films deposited with various N/C ratios in the process gas mixtures.

N/C (%)	sp^3/sp^2
0	8.5
0.4	5.5
0.6	6.2
0.8	8.4
1.0	9.0

According to the XPS analysis, the addition of ammonia to the process gas mixture can affect the chemical bonds in the deposited diamond films and increases the proportion of the diamond sp^3 phase.

3.6. Discussion

The SEM, AFM, XRD, Raman spectroscopy, and XPS characterizations described above provide notably consistent results. With the ammonia addition to the process gas mixtures at a 0.4% N/C ratio, the SEM and AFM images show that the surface is covered with many small grains. Accordingly, the XRD results indicate an increase in the FWHMs of the (111) and (220) crystals. The Raman spectra demonstrate a tendency toward graphitization. Meanwhile, the deconvolution profile from the XPS spectra illustrates an increased sp^2 fraction in the deposited film. When the N/C ratio increases from 0.6% to 0.8% and 1.0%, the SEM and AFM images show that the (110) facet grains gradually increase. Correspondingly, the XRD results indicate that the FWHMs of the (111) and (220) planes of the crystals are reduced and that the $[I_{(220)}/I_{(111)}]$ intensity ratio increases to 35.4%. The Raman spectra demonstrate an improvement in the diamond phase quality, while the deconvolution profile from the XPS spectra illustrates the increase of the sp^3 fraction in the deposited film.

Two important effects of the ammonia addition to the process gas mixtures are obvious. The first effect is the change in the crystal's preferred orientation to (100) or (110). The second effect is the increase in the sp^3 fraction. Seeking to explain the growth rate increase of the (100) or (110) grains with the N addition to the diamond film deposition process, Larsson and co-workers investigated the effect of N incorporation on the hydrogen abstraction using first-principles calculations [46]. An N atom was placed at the substitute position in different surface layers of the (100), (110), or (111) H-terminated diamond surface slabs, and the electron densities were calculated [47]. These researchers' results show that a near-surface N atom in the (100) or (110) diamond surface weakens the neighboring surface C–H bonds, thereby enhancing the rate of H-abstraction, which leads to the relatively large increase in the growth rate of the (100) or (110) grains.

The enhancement of the sp^3 phase may also be related to the adsorption, migration, and abstraction behaviors of the nitrogen atom on the diamond surface. Our investigations on this topic using the first-principles calculations are ongoing.

4. Conclusions

In this study, the effect of the ammonia addition to the process gas mixtures on diamond films was investigated through a series of MPCVD experiments and systematic characterizations. The following conclusions can be drawn:

- The addition of trace amounts of NH_3 to the standard CH_4/H_2 process gas mixture has a significant effect on the surface morphology and preferred orientation of the resulting crystals.
- Based on the XRD analysis results, ammonia addition to the process gas at a 0.4% to 1% N/C ratio causes an increase in the intensity ratios of the (220) to (111) peaks with $[I_{(220)}/I_{(111)}]$ values from 17.4% to 35.4%, indicating that a certain amount of ammonia addition to the process gas is beneficial for the growth of the (110) faceted grains.
- The XPS spectra analysis indicates that the incorporation of ammonia into the process gas can influence the sp^3 fraction of the films. The ammonia addition to the process gas at a 0.4% N/C ratio results in a decrease in the sp^3/sp^2 ratios from 8.5 to 5.5. However, upon a further increase of the ammonia addition in the N/C ratio from 0.6% to 1%, the sp^3/sp^2 ratios increase from 5.5 to 9.0, and the amount of the sp^3 phase fraction at a 1% N/C ratio exceeds the amount of the sp^3 phase fraction of undoped diamond films. This finding indicates that the ammonia addition to the process gas enhances the sp^3 fraction in the deposited diamond films.

Author Contributions: Xuejie Liu conceived and designed the experiments; Hongchao Wang performed the experiments; Pengfei Lu, Yuan Ren, Xin Tan, Shiyang Sun and Huiling Jia analyzed the data and participated in the discussions; Xuejie Liu and Hongchao Wang wrote the paper.

Acknowledgments: The authors acknowledge the financial support from the National Natural Science Foundation of China (Grant Nos. 50845065 and 51562031), the Natural Science Foundation of the Inner Mongolia Autonomous Region (Grant Nos. 2014MS0516 and 2015MS0550), and the Science and Technology Foundation of Baotou (Grant No. 2013J2001-1). The authors also thank Junyan Zhang and Yongfu Wang for their discussions regarding the Raman spectra analysis and Mingji Li for his discussions regarding the XPS spectra analysis.

Conflicts of Interest: The authors declare no conflict of interest.

References

1. Okumura, Y.; Kanayama, K.; Nishiguchi, H. Synthesis of n-type semiconducting diamond films in acetylene flame with nitrogen doping. *Proc. Combust. Inst.* **2017**, *36*, 4409–4417. [[CrossRef](#)]
2. Nemanič, V.; Žumer, M.; Kovač, J.; Koeck, F.A.M.; Nemanich, R.J. In situ reactivation of low-temperature thermionic electron emission from nitrogen doped diamond films by hydrogen exposure. *Diam. Relat. Mater.* **2014**, *50*, 151–156. [[CrossRef](#)]
3. Elfimchev, S.; Chandran, M.; Akhvlediani, R.; Hoffman, A. Visible sub-band gap photoelectron emission from nitrogen doped and undoped polycrystalline diamond films. *Appl. Surf. Sci.* **2017**, *410*, 414–422. [[CrossRef](#)]
4. Kudo, Y.; Sato, Y.; Masuzawa, T.; Yamada, T.; Saito, I.; Yoshino, T.; Chun, W.J.; Yamasaki, S.; Okano, K. Field emission from N-doped diamond doped with dimethylurea. *J. Vac. Sci. Technol. B* **2009**, *28*, 506–510. [[CrossRef](#)]
5. Skoog, S.A.; Miller, P.R.; Boehm, R.D.; Sumant, A.V.; Polsky, R.; Narayan, R.J. Nitrogen-incorporated ultrananocrystalline diamond microneedle arrays for electrochemical biosensing. *Diam. Relat. Mater.* **2015**, *54*, 39–46. [[CrossRef](#)]
6. Tong, W.; Tran, P.A.; Turnley, A.M.; Aramesh, M.; Praver, S.; Brandt, M.; Fox, K. The influence of sterilization on nitrogen-included ultrananocrystalline diamond for biomedical applications. *Mater. Sci. Eng. C* **2016**, *61*, 324–332. [[CrossRef](#)] [[PubMed](#)]
7. Tallaire, A.; Lesik, M.; Jacques, V.; Pezzagna, S.; Mille, V.; Brinza, O.; Meijer, J.; Abel, B.; Roch, J.F.; Gicquel, A.; et al. Temperature dependent creation of nitrogen-vacancy centers in single crystal CVD diamond layers. *Diam. Relat. Mater.* **2015**, *51*, 55–60. [[CrossRef](#)]
8. Seibert, W.M.; Wörner, E.; Fuchs, F.; Wild, C.; Koidl, P. Nitrogen induced increase of growth rate in chemical vapor deposition of diamond. *Appl. Phys. Lett.* **1996**, *68*, 759–760. [[CrossRef](#)]

9. Liu, T.; Raabe, D. Influence of nitrogen doping on growth rate and texture evolution of chemical vapor deposition diamond films. *Appl. Phys. Lett.* **2009**, *94*, 021119. [[CrossRef](#)]
10. Tang, C.J.; Fernandes, A.J.S.; Granada, M.; Leitao, J.P.; Pereira, S.; Jiang, X.F.; Pinto, J.L.; Ye, H. High rate growth of nanocrystalline diamond films using high microwave power and pure nitrogen/methane/hydrogen plasma. *Vacuum* **2015**, *122*, 342–346. [[CrossRef](#)]
11. Jin, S.; Moustakas, T.D. Effect of nitrogen on the growth of diamond films. *Appl. Phys. Lett.* **1994**, *65*, 403–405. [[CrossRef](#)]
12. Samlenski, R.; Haug, C.; Brenn, R.; Wild, C.; Lecher, R.; Koidl, P. Characterisation and lattice location of nitrogen and boron in homoepitaxial CVD diamond. *Diam. Relat. Mater.* **1996**, *5*, 947–951. [[CrossRef](#)]
13. Lecher, R.; Wild, C.; Herres, N.; Behr, D.; Koidl, P. Nitrogen stabilized (100) texture in chemical vapor deposited diamond films. *Appl. Phys. Lett.* **1994**, *65*, 34–36. [[CrossRef](#)]
14. Bergmaier, A.; Dollinger, G.; Faestermann, T.; Frey, C.M.; Ferguson, M.; Güttler, H.; Schulz, G.; Willerscheid, H. Detection of nitrogen in CVD diamond. *Diam. Relat. Mater.* **1996**, *5*, 995–997. [[CrossRef](#)]
15. Cao, G.Z.; Schermer, J.J.; Van Enckevort, W.J.P.; Elst, W.A.L.M.; Giling, L.J. Growth of {100} textured diamond films by the addition of nitrogen. *J. Appl. Phys.* **1996**, *79*, 1357–1364. [[CrossRef](#)]
16. Chatei, H.; Bougdira, J.; Remy, M.; Alnot, P. Mechanisms of diamond films deposition from MPACVD in methane-hydrogen and nitrogen mixtures. *Surf. Coat. Technol.* **1998**, *98*, 1013–1019. [[CrossRef](#)]
17. Tang, C.J.; Fernandes, A.J.S.; Costa, F.; Pinto, J.L. Effect of microwave power and nitrogen addition on the formation of (100) faceted diamond from microcrystalline to nanocrystalline. *Vacuum* **2011**, *85*, 1130–1134. [[CrossRef](#)]
18. Othman, M.Z.; May, P.W.; Fox, N.A.; Heard, P.J. Incorporation of lithium and nitrogen into CVD diamond thin films. *Diam. Relat. Mater.* **2014**, *44*, 1–7. [[CrossRef](#)]
19. Ullah, M.; Ahmed, E.; Welch, K.; Majdi, S.; Khalid, N.R.; Ahmad, M. Growth of Nitrogen-Incorporated Diamond Films Using Hot-Filament Chemical Vapor Deposition Technique. *Adv. Sci. Lett.* **2013**, *19*, 291–295. [[CrossRef](#)]
20. Cherf, S.H.; Chandran, M.; Michaelson, S.H.; Elfimchev, S.; Akhvlediani, R.; Hoffman, A. Nitrogen and hydrogen content, morphology and phase composition of hot filament chemical vapor deposited diamond films from $\text{NH}_3/\text{CH}_4/\text{H}_2$ gas mixtures. *Thin Solid Films* **2017**, *638*, 264–268. [[CrossRef](#)]
21. Chatei, H.; Bougdira, J.; Remy, M.; Alnot, P.; Bruch, C.; Krueger, J.K. Effect of nitrogen concentration on plasma reactivity and diamond growth in a $\text{H}_2\text{-CH}_4\text{-N}_2$ microwave discharge. *Diam. Relat. Mater.* **1997**, *6*, 107–119. [[CrossRef](#)]
22. Liu, X.; Yin, Y.; Ren, Y.; Wei, H. Adsorption and evolution behavior of $4\text{C}1\text{Si}$ island configurations on diamond (001) surface: A first principle study. *J. Alloy. Compd.* **2015**, *618*, 516–521. [[CrossRef](#)]
23. Liu, X.; Qiao, H.M.; Kang, C.J.; Ren, Y.; Tan, X.; Sun, S.Y. Adsorption and migration behavior of Si atoms on the hydrogen-terminated diamond (001) surface: A first principles study. *Appl. Surf. Sci.* **2017**, *420*, 542–549. [[CrossRef](#)]
24. Liu, X.; Kang, C.J.; Qiao, H.M.; Ren, Y.; Tan, X.; Sun, S.Y. Theoretical Studies of the Adsorption and Migration Behavior of Boron Atoms on Hydrogen-Terminated Diamond (001) Surface. *Coatings* **2017**, *7*, 57.
25. Liu, X.; Luo, H.; Ren, Y.; Xia, Q.; Li, W.; Tan, X.; Sun, S. Theoretical study of the migration behaviour of Y-C atoms on diamond (001) surface. *Diam. Relat. Mater.* **2016**, *61*, 102–108. [[CrossRef](#)]
26. Liu, X.; Li, W.; Ren, Y.; Luo, H.; Xia, Q.; Tan, X.; Sun, S. Adsorption and migration behaviours of Nb-C atoms on clean diamond (001) surface: A first principles study. *Comp. Mater. Sci.* **2016**, *121*, 159–166. [[CrossRef](#)]
27. Liu, X.; Lu, P.; Wang, H.; Ren, Y.; Tan, X.; Sun, S. Morphology and structure of Ti-doped diamond films prepared by microwave plasma chemical vapor deposition. *Appl. Surf. Sci.* **2018**, *442*, 529–536. [[CrossRef](#)]
28. Truscott, B.S.; Kelly, M.W.; Potter, K.J.; Johnson, M.; Ashfold, M.N.R. Microwave plasma-activated chemical vapour deposition of nitrogen-doped diamond. I. N_2/H_2 and NH_3/H_2 plasmas. *J. Phys. Chem. A* **2015**, *120*, 8537–8549. [[CrossRef](#)] [[PubMed](#)]
29. Truscott, B.S.; Kelly, M.W.; Potter, K.J.; Ashfold, M.N.R. Microwave plasma-activated chemical vapor deposition of nitrogen-doped diamond. II: $\text{CH}_4/\text{N}_2/\text{H}_2$ plasmas. *J. Phys. Chem. A* **2016**, *120*, 8537–8549. [[CrossRef](#)] [[PubMed](#)]
30. May, P.W.; Burrige, P.R.; Rego, C.A.; Tsang, R.S.; Ashfold, M.N.R.; Rosser, K.N.; Tanner, R.E.; Cherns, D.; Vincent, R. Investigation of the addition of nitrogen-containing gases to a hot filament diamond chemical vapour deposition reactor. *Diam. Relat. Mater.* **1996**, *5*, 354–358. [[CrossRef](#)]

31. Wang, Y.J.; Li, J.X.; Long, H.Y.; Luo, H.; Zhou, B.; Xie, Y.N.; Li, S.S.; Wei, Q.P.; Yu, Z.M. A periodic magnetic field assisted chemical vapor deposition technique to fabricate diamond film with preferred orientation. *Surf. Coat. Technol.* **2016**, *292*, 49–53. [[CrossRef](#)]
32. Tang, C.J.; Neves, A.J.; Pereira, S.; Fernandes, A.J.S.; Grácio, J.; Carmo, M.C. Effect of nitrogen and oxygen addition on morphology and texture of diamond films (from polycrystalline to nanocrystalline). *Diam. Relat. Mater.* **2008**, *17*, 72–78. [[CrossRef](#)]
33. Rakha, S.A.; Zhou, X.T.; Zhu, D.Z.; Yu, G.J. Effects of N₂ addition on nanocrystalline diamond films by HFCVD in Ar/CH₄, gas mixture. *Curr. Appl. Phys.* **2010**, *10*, 171–175. [[CrossRef](#)]
34. Ferrari, A.C.; Robertson, J. Resonant Raman spectroscopy of disordered, amorphous, and diamond like carbon. *Phys. Rev. B* **2001**, *64*, 075414. [[CrossRef](#)]
35. Ferrari, A.C.; Robertson, J. Interpretation of Raman spectra of disordered and amorphous carbon. *Phys. Rev. B* **2000**, *61*, 14095–14107. [[CrossRef](#)]
36. Klauser, F.; Steinmüller-Nethl, D.; Kaindl, R.; Bertel, E.; Memmel, N. Raman studies of nano- and ultra-nanocrystalline diamond films grown by hot-filament CVD. *Chem. Vap. Depos.* **2010**, *16*, 127–135. [[CrossRef](#)]
37. Vlasov, I.I.; Goovaerts, E.; Ralchenko, V.G.; Konov, V.I.; Khomich, A.V.; Kanzyuba, M.V. Vibrational properties of nitrogen-doped ultrananocrystalline diamond films grown by microwave plasma CVD. *Diam. Relat. Mater.* **2007**, *16*, 2074–2077. [[CrossRef](#)]
38. Praver, S.; Nemanich, R.J. Raman spectroscopy of diamond and doped diamond. *Philos. Trans. R. Soc. A Math. Phys. Eng. Sci.* **2004**, *362*, 2537–2565. [[CrossRef](#)] [[PubMed](#)]
39. Stuart, S.-A.; Praver, S.; Weiser, P.S. Growth-sector dependence of fine structure in the first-order Raman diamond line from large isolated chemical-vapor-deposited diamond crystals. *Appl. Phys. Lett.* **1993**, *62*, 1227–1229. [[CrossRef](#)]
40. Safaie, P.; Eshaghi, A.; Bakhshi, S.R. Structure and mechanical properties of oxygen doped diamond-like carbon thin films. *Diam. Relat. Mater.* **2016**, *70*, 91–97. [[CrossRef](#)]
41. Ferro, S.; Colle, M.D.; Battisti, A.D. Chemical surface characterization of electrochemically and thermally oxidized boron-doped diamond film electrodes. *Carbon* **2005**, *43*, 1191–1203. [[CrossRef](#)]
42. Jia, F.; Bai, Y.; Qu, F.; Zhao, J.; Zhuang, C.; Jiang, X. Effect of B/C ratio on the physical properties of highly boron-doped diamond films. *Vacuum* **2010**, *84*, 930–934. [[CrossRef](#)]
43. Sheng, Z.H.; Shao, L.; Chen, J.J.; Bao, W.J.; Wang, F.B.; Xia, X.H. Catalyst-free synthesis of nitrogen-doped graphene via thermal annealing graphite oxide with melamine and Its excellent electrocatalysis. *ACS Nano* **2011**, *5*, 4350–4358. [[CrossRef](#)] [[PubMed](#)]
44. Sun, Q.; Wang, J.H.; Weng, J.; Liu, F. Surface structure and electric properties of nitrogen incorporated NCD films. *Vacuum* **2017**, *137*, 155–162. [[CrossRef](#)]
45. Li, Y.L.; Li, J.J.; Xia, X.X.; Lu, C.; Jin, H.; Gu, C.Z. Effect of grain boundary on local surface conductivity of diamond film. *J. Appl. Phys.* **2009**, *105*, 013706. [[CrossRef](#)]
46. Regemorter, T.V.; Larsson, K. A Theoretical study of nitrogen-induced effects on initial steps of diamond CVD growth. *Chem. Vap. Depos.* **2008**, *14*, 224–231. [[CrossRef](#)]
47. Yiming, Z.; Larsson, F.; Larsson, K. Effect of CVD diamond growth by doping with nitrogen. *Theor. Chem. Acc.* **2014**, *133*, 1432. [[CrossRef](#)]

